Edge detection in two-dimensional images through model polynomial fitting and first order derivative

Genta Mirku, Nolla Sherifi, Carlo Ciulla*, Sindi Dhima and Nikol Zaçe

Department of Computer Engineering,
Epoka University,
Rr. Tiranë-Rinas, Km. 12, 1032, Vorë, Tirana, Albania
Email: gmirku17@epoka.edu.al
Email: nsherifi17@epoka.edu.al
Email: cciulla@epoka.edu.al
Email: cxc2728@njit.edu
Email: sdhima17@epoka.edu.al
Email: nzace17@epoka.edu.al
*Corresponding author

Abstract: An innovative edge detection method based on model polynomial fitting and calculation of first order derivative of two-dimensional images is here proposed. The two partial first order derivatives of the model function are calculated. The square root of the sum of the squares of the partial first order derivatives is called FOD and is calculated at the intra-pixel point (x, y). The image is thus re-sampled using the surface of the FOD. The methodology is tested with theoretical images and with Magnetic Resonance Images. Results are compared within a set of five model polynomial functions designed to have three gradients: two along the main spatial coordinates; and one along the covariate direction. FOD images provide clear and sharp edges and similar edge detection behaviour. The implications of this methodology are in image processing and more specifically in edge detection. The advantage of the method is to be computationally fast.

Keywords: model polynomial function; first order derivative; FOD; gradient; edge detection.

Reference to this paper should be made as follows: Mirku, G., Sherifi, N., Ciulla, C., Dhima, S. and Zaçe, N. (2022) 'Edge detection in two-dimensional images through model polynomial fitting and first order derivative', *Int. J. Student Project Reporting*, Vol. 1, No. 1, pp.3–24.

Biographical notes: Genta Mirku received her Bachelor's in Computer Engineering from Epoka University, Tirana, Albania in 2020. During the years 2019 and 2020, she has followed two internships as a web developer intern and TIBCO developer intern. Her academic interests are in programming, data science, artificial intelligence and image processing.

Nolla Sherifi received her BS in Computer Engineering from Epoka University, Tirana, Albania in 2020. Throughout her college life, she joined many programming activities and worked as a volunteer in Charlevoix Public Library to coordinate libraries' support services. She plans to pursue her Master's in Software Engineering.

Carlo Ciulla's former academic appointments were as Science and Technology Agency Fellow (STA) at the National Institute of Bioscience and Human Technology in Tsukuba – Japan (1995–1997), graduate student at RUTGERS and NJIT (1998–2002), research associate at Yale University (2002–2003), postdoctoral scholar at the University of Iowa (2004–2005), postdoctoral scholar at Wayne State University (2005–2007) and Assistant Professor of Computer Science at Lane College (2007–2009). During the years 2009 to 2012, he had been a self-employed scholar whom devoted his time to his research interests related to the development of innovative methods of signal interpolation and also to the development of educational software for students. In 2012, he joined the University of Information Science and Technology (UIST) St. Paul the Apostle, Ohrid, Republic of North Macedonia, as an Assistant Professor. In 2019, he joined Epoka University's Department of Computer Engineering as a Lecturer and Associate Professor.

Sindi Dhima received her BSc in Computer Engineering from Epoka University, Tirana, Albania in 2020. Her research interests span across the disciplines of signal processing, computer vision, data science, machine learning, and artificial intelligence.

Nikol Zaçe received her BSc in Computer Engineering from Epoka University, Tirana, Albania in 2020. Her research interests span the domain of model polynomial fitting and FOD-based approaches to image processing and edge detection.

1 Introduction

1.1 Significance of edge detection

Computer vision encompasses a wide array of disciplines and since its inception has been object of study by many researchers. One area of application of computer vision is edge detection. This application embeds a great significance in image processing. The basic idea in edge detection is the extraction of boundaries existing between objects that are imaged and represented in digital form. Normally, an edge is a high frequency component of an image and that is because the gradient of the signal in between two objects is a spike signal with abrupt passage from one value to another value. Low frequency components identifiable as noise are also likely to be in the image to process. That is why many algorithms for edge detection start processing the image with a threshold operation that achieves to select the image points which are candidate edges and to separate them from image points that are not edges. The detection of an object or a surface in a digital image is pivotal in image segmentation (Dolz et al., 2015). Indeed, many image processing algorithms in magnetic resonance image processing depart from segmented image which represent the object surface to be used for further processing. This paper acknowledges the significance of edge detection in magnetic resonance imaging (MRI) and proceeds in the next sections to explore the state of the art and to present a novel technique which is based on model polynomial fitting (Ciulla et al., 2015) and calculation of first order derivative (FOD) for edge detection (Yahaya, 2017). The application of edge detection in this paper is through FOD of the model polynomial function fitted to image data, and is geared to demonstrating feasibility when using

theoretical images and also magnetic resonance images. A characteristic problem of edge detection in MRI is noise. Since its inception, edge detection has been developed to avoid that noise would become a confounding factor when choosing image points as edges candidates. The most immediate solution to this problem is the use of gradients to process the image objects and surfaces. A gradient is sensitive to a change in pixel intensity and as such is a well-behaved instrument to detect both noise and edge points. There is need of a criterion in order to distinguish between gradients of noise signal and gradients of edge signal. The literature reports that threshold is a valuable option to perform such distinction. It will become manifest through this paper that the technique here proposed does not make use of preprocessing operations as threshold because of the mathematical nature of the model function chosen to be fitted to images. The nature of the model functions here presented is such to devise three gradients: one along the spatial coordinate 'x', one along the spatial coordinate 'y' and one along the covariate direction 'x y'. By doing so, to survive the gradients, noise needs to persist in 'x' and 'y' directions simultaneously. If otherwise, noise is detectable along the three directions simultaneously is then featured as if it was signal. Figures 2, 3 and 4 illustrate this concept and open up to the presentation of the edge detection technique here proposed.

1.2 Discussion of the state of the art

Since its inception, edge detection has been driven by pioneering techniques that approximate the FOD of the image. These techniques rely on convolution masks used to filter the image. The most important of these techniques are Roberts, Prewitt and Sobel operators (Roberts, 1963; Prewitt, 1970; Sobel, 1990). In their simple most inception these operators were one dimensional arrays of convolving factors covering 'x' and 'y' direction separately, thus to cover the diagonal direction 'x y' these operators evolved into two-dimensional masks. A common procedure adopted by these methods was to filter the image through convolution mask so to approximate the FOD. Then, it follows computation of gradient magnitude image, and threshold the gradient magnitude image so to obtain output binary image (Spontón and Cardelino, 2015).

Algorithms that have evolved from the pioneer methods are based on calculation of second order derivative of the image. They generally employ a preprocessing step aimed to reduce noise in the image. Marr-Hildreth algorithm is based on finding zero crossing points of second order derivative of the image (Spontón and Cardelino, 2015). The algorithm proposes the use of Gaussian smoothing operator to filter the high-frequency noise and then uses Laplacian operator for edge detection (Marr and Hildreth, 1980). In practice, the first step consists of convolving the image with Laplacian of Gaussian (LoG) operator, or in alternative the image is first convolved with the Gaussian kernel and then convolved with the Laplacian operator. The second step involves the search for zero crossing points in the filtered image, which is a threshold operation that outputs the final binary image comprising of the edges (Spontón and Cardelino, 2015).

Haralick's (1984) method is also based on the idea to find zeros in the second order derivative of the image. The approach is however carried out with model polynomial fitting. In the specifics, the author fits a bi-cubic polynomial to the image and then equates to zero the second order derivative of the polynomial. By doing so, is possible to obtain the constraint to enforce in order to find the zeros in the second order derivative of the image. According to Haralick's definition, a pixel will be an edge if the following three conditions hold true:

1 the FOD is non-zero

2 the second order derivative is zero

3 the third order derivative is negative (Spontón and Cardelino, 2015).

Haralick's method is not quite the same as our method for what pertains the polynomial model fitting. Normally, the determination of the polynomial coefficient requires a larger number of data points so that the resulting nonlinear system is over-determined and requires least-square solutions, which are solved through convolutions of the image with masks. As opposed to Haralick's method, our method fits locally (pixel-by-pixel) a model polynomial function. Then it calculates the first order partial derivatives of the model function, and it calculates the magnitude of the FOD, which is the edge detection image.

In Canny's edge detection idea, edges are marked at maxima in gradient magnitude of Gaussian-smoothed image. The detection problem starts with an edge which is bathed in white Gaussian noise. The edge is convolved with a filter having impulse response: a difference of boxes operator; or a FOD of the Gaussian operator. The results of these two convolutions are marked at the local maximum, and the local maximum is marked as the centre of an edge (see Figure 1 in Canny, 1986).

Current trends indicate that edge detection and more generally object recognition is achieved with convolutional neural networks (CNNs) within the deep learning framework (Zhao et al., 2019). Moreover, edge detection can be attained with dilated convolutions networks (as opposed to deeper CNNs), which keep the spatial resolution of the image while encoding the edge information (He et al., 2019). The advantage of CNNs approaches is to avoid extracting features from the images and to use high level information readily available when coding the image in full into the network (Liu et al., 2017). A drawback of the use of CNNs for edge detection is determined when the image includes small perturbations, which may cause holistic edge detection methods to be unsuccessful (Xie and Tu, 2015; Cosgrove and Yuille, 2020). Edge detection can also be achieved by inverse Fourier transformation of images pre-processed with phase-shifting techniques (Ren et al., 2018). The literature also reports on metrics for quality assessment of edge detection (Sadykova and James, 2017). To alleviate false edge detection is possible with preprocessing steps that smooth the image with Gaussian kernels (Zhang et al., 2017). Smoothing determines noise suppression and that is important in diagnostic settings.

1.3 The presentation of our method

Digital images can be represented and stored as matrices of values: the pixel intensity values. This property makes it possible to use images in computing through image processing algorithms. Image processing is the science that develops computational methodologies used to extract useful information from the images. Processing of the images is done through numerous algorithms based on the goal to achieve. Digital image processing has thus many fields of application. One of the most common and useful is the biomedical imaging field like MRI. There is an immense literature on image processing in MRI. In this field the most important applications are: segmentation, to extract a boundary or a surface (Khin et al., 2020); registration, to align images acquired at different time frames (Wang and Li, 2019); and computing performed with the aim to extract information from the images (Bryan et al., 2020).

One important technique in image processing is edge detection because makes it possible to filter the edge between surfaces represented by the images. Due to this impact, many edge detection algorithms have been developed throughout the years (Jain et al., 1995; James, 2016). Edges consist of meaningful features and contain significant information such as the boundary between surfaces. Indeed, two regions of an image may be characterised by different brightness levels, which correspond to a change in pixel intensity. The change may be the indicator of the borderline between surfaces (discontinuity) and can be detected through the calculation of the FOD. A location with coordinates (x, y) in the image, which belongs to the border between regions of the image displaying different brightness, is called an edge point. An algorithm, or more generally a method, that can detect the change of pixel intensity between regions and highlight the edges between regions of the image is usually called edge detector. Edge detection is one fundamental research area within the wide array of subjects covered in computer vision. The precursors of edge detection were Canny, Roberts, Sobel and Prewitt (Roberts, 1963; Prewitt, 1970; Canny, 1986; Sobel, 1990). In recent times the use of model fitting and the consequential calculation of the FOD of the image data has been explored and also compared to Sobel and Prewitt edge detection (Yahaya, 2017).

This paper proposes five polynomial functions (among which is the bivariate linear) as models to fit the pixels of the image, so to enforce continuity within the pixel and to allow re-sampling. The rationale of this work is to estimate the edges in the image. In order to do so, model fitting provides a viable option. The FOD of the model function is then revealed to be the edge finder image. The FOD is calculated as the square root of the sum of the squares of the two first order partial derivatives respect to the two spatial coordinates x and y. The important and relevant feature of the model function is the gradient properties embedded through the calculation of finite differences between adjacent pixels along the two spatial coordinates and also the gradient that measures the covariation of the image pixels along x and y directions simultaneously. The mathematics of the methodology here proposed is illustrated in the theory section. The paper also presents validation through study of edge detection properties of the model functions and shows them to have similar properties.

As classifiable as methodology requiring the calculation of FOD of an image, our methodology does not require threshold of the FOD magnitude. Roberts, Prewitt and Sobel methods approximate the FOD of the image. Then, threshold that image. In our methodology, threshold is not required, thus the edge detection phase consists in the calculation of FOD. The aforementioned methods use the threshold phase as a selective process which determines as to if an image point is an edge or not. Conversely, our method uses the FOD image as the result of the edge detection process. Along this line of thought our procedure makes a difference also with Canny's hysteresis threshold (Canny, 1986), by means of which, a point is accepted as candidate edge if it is above an upper threshold or if it is above a lower threshold and connected to a surface located above the upper threshold. The advantage is clearly that our methodology does not depend on arbitrary thresholds. Another interesting aspect that relates to our methodology is the model fitting procedure, which is not novel in literature as it was introduced for edge detection in Haralick's paper (1984). However, due to the over-determined non-linear system to be solved when using Haralick's approach, least square solutions need to use convolving masks, which determine the edges of the image. Therefore, our approach combines model polynomial fitting with calculation of FOD image, and it is a unique

approach which was recently initiated in the literature (Yahaya, 2017) and expanded here to a larger number of model polynomial functions.

2 Theory

To calculate the FOD of an image on a pixel-by-pixel basis is possible after model polynomial fitting. A 2 × 2 neighbourhood of pixels provides the model function the property to embed three gradients. The gradients are finite differences between pixel intensity values in the neighbourhood. One gradient is calculated along each of the two spatial directions x and y, and one gradient measures the covariation of pixel intensity values along the diagonal direction ('xy'). The model function is designed to act as a high pass filter. Thus, the function allows passing spikes of the signal corresponding to the gradient existing between surfaces of the image, and rejects adjacent pixels with similar or same brightness value. The result is an edge finder image. This section presents the math of the bivariate linear model polynomial function [SRE2D(x, y) in equation (1)] and the set of model polynomial functions that were chosen for this study [see equations (2), (3), (4) and (5)].

$$\mathrm{SRE2D}(x, y) = f(0, 0) + \theta_x \cdot x + \theta_y \cdot y + \omega_f \cdot xy \tag{1}$$

$$\begin{aligned} g(x, y) = f(0, 0) &+ \theta_x \cdot a\left[(x+y)^3 + 2(x+y)^2 + (x+y) + 1\right] \\ &+ \theta_y \cdot b\left[(x+y)^2 + (x+y) + 1\right] + \omega_f \cdot c(x+y) \end{aligned} \tag{2}$$

$$\begin{aligned} s(x, y) = f(0, 0) &+ \theta_x \cdot \left[(x-a)^2 + (y-b)^2\right] + \theta_y \cdot \left[(a-x)^2 + (b-y)^2\right] \\ &+ \omega_f \cdot c(x+y) \end{aligned} \tag{3}$$

$$h(x, y) = f(0, 0) + \theta_x \cdot \left[(x+a)^2\right] + \theta_y \cdot \left[(y+b)^2\right] + \omega_f \cdot c(x+y) \tag{4}$$

$$f(x, y) = f(0, 0) + \theta_x \cdot \left(ax^2 + x + 1\right) + \theta_y \cdot (by^2 + y + 1) + \omega_f \cdot (x+y) \tag{5}$$

$f(0, 0)$ is the pixel intensity value to re-sample through the model function and θ_x, θ_y, ω_f, a, b and c are constants.

$$\theta_x = f(1, 0) - f(0, 0) \tag{6}$$

$$\theta_y = f(0, 1) - f(0, 0) \tag{7}$$

$$\omega_f = f(1, 1) + f(0, 0) - f(1, 0) - f(0, 1) \tag{8}$$

We obtain these results:

$$\left(\partial\left(\mathrm{SRE2D}(x, y)\right)\right)/\partial x = \theta_x + y \cdot \omega_f \tag{9}$$

$$\left(\partial\left(\mathrm{SRE2D}(x, y)\right)\right)/\partial y = \theta_y + x \cdot \omega_f \tag{10}$$

$$\left(\partial\left(g(x, y)\right)/\partial x\right) = \theta_x \cdot a\left[3(x+y)^2 + 4(x+y) + 1\right] + \theta_y \cdot b\left[2(x+y) + 1\right] + \omega_f \cdot c \tag{11}$$

$$\left(\partial\left(g(x,\ y)\right)/\partial y\right)=\theta_x\cdot a\left[3(x+y)^2+4(x+y)+1\right]+\theta_y\cdot b\left[2(x+y)+1\right]+\omega_f\cdot c \quad (12)$$

$$\left(\partial\left(s(x,\ y)\right)/\partial x\right)=2\left[\theta_x\cdot(x-a)+\theta_y\cdot(x-a)\right]+\omega_f\cdot c \quad (13)$$

$$\left(\partial\left(s(x,\ y)\right)/\partial y\right)=2\left[\theta_x\cdot(y-b)+\theta_y\cdot(y-b)\right]+\omega_f\cdot c \quad (14)$$

$$\left(\partial\left(h(x,\ y)\right)/\partial x\right)=2\cdot\theta_x\cdot(x+a)+\omega_f\cdot c \quad (15)$$

$$\left(\partial\left(h(x,\ y)\right)/\partial y\right)=2\cdot\theta_y\cdot(y+b)+\omega_f\cdot c \quad (16)$$

$$\left(\partial\left(f(x,\ y)\right)/\partial x\right)=\theta_x\cdot(2ax+1)+\omega_f \quad (17)$$

$$\left(\partial\left(f(x,\ y)\right)/\partial y\right)=\theta_y\cdot(2by+1)+\omega_f \quad (18)$$

The magnitude of FOD of the image is:

$$FOD(x,\ y)=\sqrt{\left[\left(\partial\,\Phi(x,\ y)/\partial x\right)\right]^2+\left[\left(\partial\,\Phi(x,\ y)/\partial y\right)\right]^2} \quad (19)$$

$\Phi(x,\ y)$ is either of the model polynomial functions in equations (1) through (5). Constants a, b and c were chosen in order to obtain an image that actually acts as an edge finder. Tests were conducted with a set of numbers in the range [–2.5, 2.5] and it was observed that, with the increment of the absolute values of the constants, the edges on the FOD images became sharper. However, this effect was detected up to some point after which, increasing or decreasing the values did yield no difference. The values were set the same in order to give to all of the three gradients the same level of activity.

3 Results

3.1 Experimental determination of the constants of the model polynomial functions

Preliminary investigation was conducted in order to study the effect of the constants of the polynomial model functions. The function g(x, y) was chosen for this study. Generally when the constant is zero, the corresponding gradient is nullified and so the effect is to truncate the edge finding properties of FOD derived from the function. The interval of study was kept in the values between [–2.5, 2.5]. The FOD images were calculated at steps of 0.5, from –2.5 to 2.5 for all of the three constants. A total of 33 images were obtained and analysed. The best images are reported in Figure 1. The picture shows the effect of the nullification of the gradient along ‘x’ and the gradient along ‘y’. It also shows that if the two gradients along ‘x’ and ‘y’ are kept (value of the constants non zero), and if the gradient along the covariate direction ‘x y’ is nullified, the edges are found anyway. Overall, this study confirms that when the values of ‘a’, ‘b’ and ‘c’ are the same, most uniform edge finding properties are observable.

Figure 1 Edge finder behaviour of g(x, y) model polynomial function on rectangle image

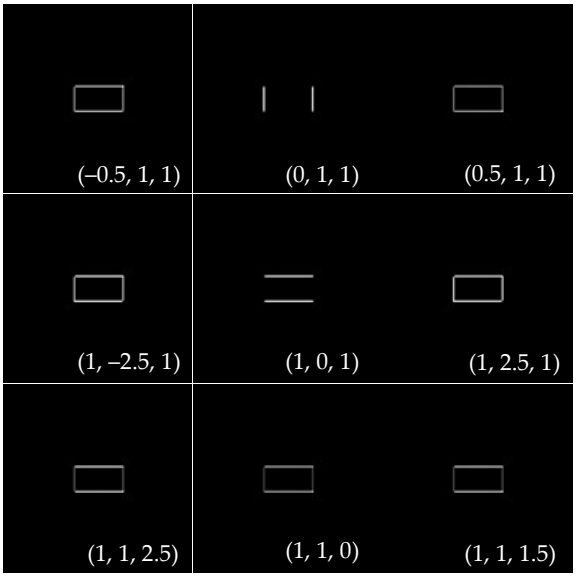

Notes: Noticeably, when a = 0 horizontal edges are not found [see image labelled with (0, 1, 1)]. When b = 0 vertical edges are not found [see image labelled with (1, 0, 1)]. In all the other cases, the four edges are well defined. Worth noting that when the value of c = 0 [see image labelled with (1, 1, 0)] the four edges are found because 'a' and 'b' are non-null.

3.2 Analysis of the robustness to noise

Noise was artificially created and introduced into the images to test the method for its robustness. Two types of noise were calculated: Gaussian and sinusoidal. Gaussian noise had standard deviation set to 2.0. Both Gaussian and sinusoidal noise had a multiplicative factor that could be tuned to obtain the desired levels. The factor was set to 500, 1,000 and 2,000 for the Gaussian and 50, 100 and 200 for the sinusoidal waves. Figure 2 shows noise, images with sinusoidal noise added to them, and FODs. From the two rows from the top and for each couple of rows, the picture shows an experimental session. FOD images were calculated for both noise and images. From top to bottom and for each couple of rows, model polynomial functions were: s(x, y), f(x, y), g(x, y).

Similarly, Figure 3 show two experimental sessions as relevant to Gaussian noise. The FOD images in Figure 2 and 3 show that noise can be detected and featured in its spatial shape by the FOD images. The cases for which the FOD is not affected by the noise (it is robust to noise) are indicated by noise level in yellow colour. Figure 4 show an experimental session utilising real MRI data. From left to right the picture shows the noise, the noisy image and the FOD of the noisy image. The noise was raised to the level of maximal tolerability which is 1000 for Gaussian noise and 15 for sinusoidal noise. After these levels the noise is featured in the FODs and its edges are reconstructed. In Figure 4, the model polynomial function is SRE2D(x, y).

Figure 2 Sinusoidal noise (see online version for colours)

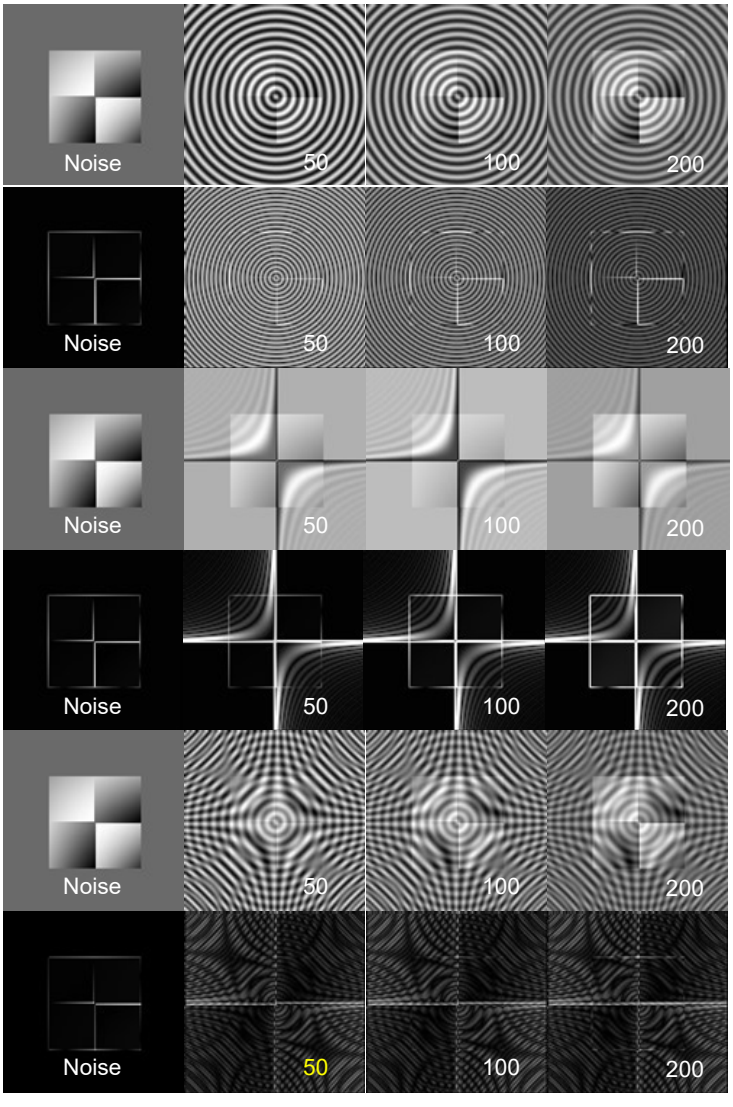

Notes: From the two top rows, from left to right: noise, three images with noise levels: 50, 100 and 200. FOD of the noise image, FODs of the noisy images (in second, fourth and sixth rows from the top). The model polynomial function is s(x, y) in first and second rows from the top; f(x, y) is the model polynomial function used in third and fourth rows from the top; and g(x, y) in the two bottom rows. Values of constants were [a, b, c] = [2.5, 2.5, 2.5]. The FOD images show both robustness to noise in one case (see noise level in yellow colour) and also that the noise can be featured and detected in its spatial extent. Sinusoidal noise is one of the most difficult noises to deal with if the frequency is not known and if the amplitude is low.

Figure 3 Gaussian noise (see online version for colours)

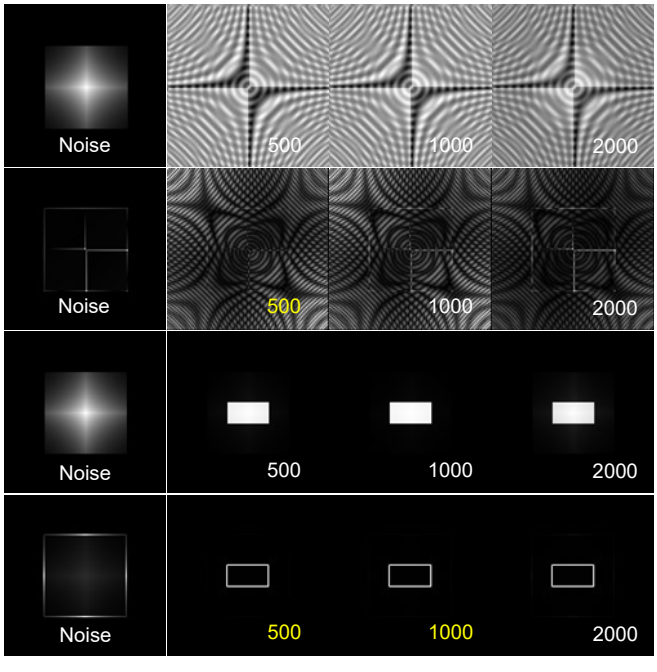

Notes: From left to right, in the two rows from the top the picture shows noise, three noisy images with noise levels: 500, 1,000 and 2,000, and FODs (in second and fourth row from the top). The model polynomial function is h(x, y) and values of constants were [a, b, c] = [2.5, 2.5, 2.5]. The FOD images show both robustness to noise (see noise level in yellow colour) and also that the noise can be featured and detected in its spatial extent.

Figure 4 In each row, from left to right: Gaussian noise, noisy MRI and FOD of the noisy MRI

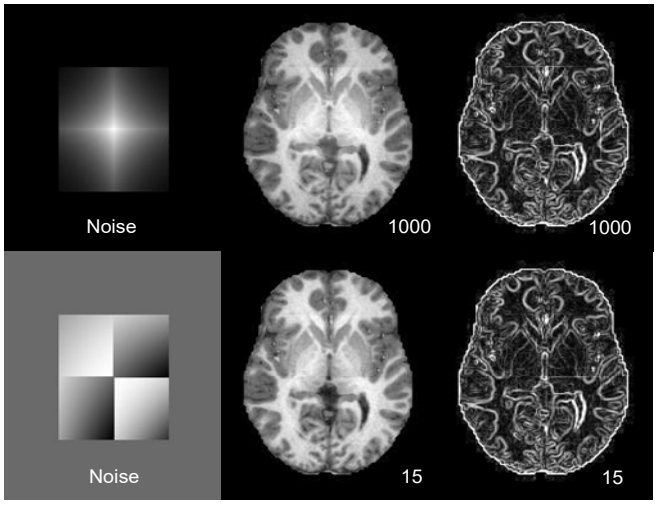

Note: Noise levels (1,000 for Gaussian noise and 15 for sinusoidal noise) were set to test the robustness. The model polynomial function was SRE2D(x, y).

3.3 Validation

The rationale of the validation is to ascertain that the SRE2D and the other functions offer similar edge detection performance. The assumption is justified by the fact that all of the functions possess three gradients (along 'x', along 'y' and along the covariate direction 'xy') and thus their FODs are expected to show similar characteristics as edge detectors. The validation of the assumption was conducted using the FODs as edge detector in a test set of magnetic resonance images across various modalities (T1-weighted, T2-weighted, and angiography).

Figure 5 MRI (OASIS database) in (a). FOD calculated with h(x, y) in (b), (c), (d) and (e)

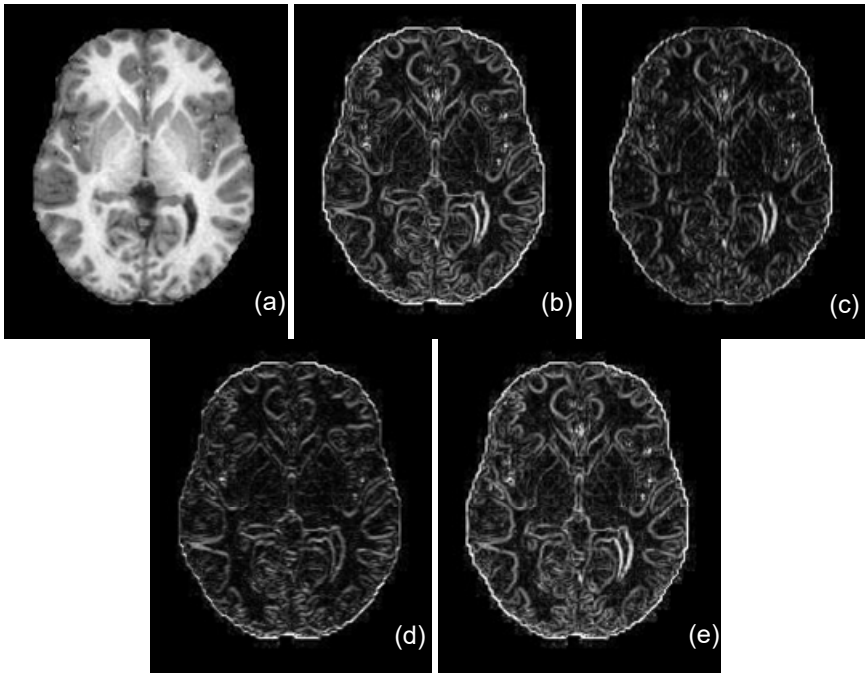

Note: The values of the constants were: (a, b, c) = (1.0, 1.0, 1.0) in (b); (a, b, c) = (0.0, 1.0, 1.0) in (c); (a, b, c) = (1.0, 0.0, 1.0) in (d); and (a, b, c) = (0.0, 0.0, 1.0) in (e).

Figure 5 gives an illustration of the FOD image [see (b)] of an MRI (a) obtained using h(x, y) as model function [equation (4)] and shows that best results are obtained when the three gradients and all equally active [see (b)]. Figure 6 shows some set results obtained using theoretical images fitted with four model functions [see equations (2), (3), (4) and (5)]. Figure 6 also shows the kurtosis (Caviedes and Gurbuz, 2002) of each theoretical image. Kurtosis was adopted to be the direct measure of image brightness and so results of FOD and kurtosis are compared. The expectation from FODs is to have brighteness topography as close as possible to kurtosis, so to have confirmation of effective edge detection. Figure 6 shows that the expectation on the FODs is met given their topography so closely matching the topography of kurtosis images. The error measure: sum of squared differences (SSD) between FOD and kurtosis; is displayed in the bottom row in Figure 6. SSD images were calculated after binarisation of FOD and kurtosis images, and

they were zero except for those shown in (p), (q) as relevant to the rectangle [see top row, (a)] and the sinc signal [see fourth row from the top, (j)].

Figure 6 Theoretical images in (a), (d), (g), (j) and (m); FOD calculated with f(x, y) in (b); FOD calculated with g(x, y) in (e); FOD calculated with h(x, y) in (h). FOD calculated with s(x, y) in (k); FOD calculated with g(x, y) in (n); kurtosis of theoretical images in: (c), (f), (i), (l) and (o); SSD images in (p), (q), as relevant to the cases presented in the first row from the top and the fourth row from the top
(see online version for colours)

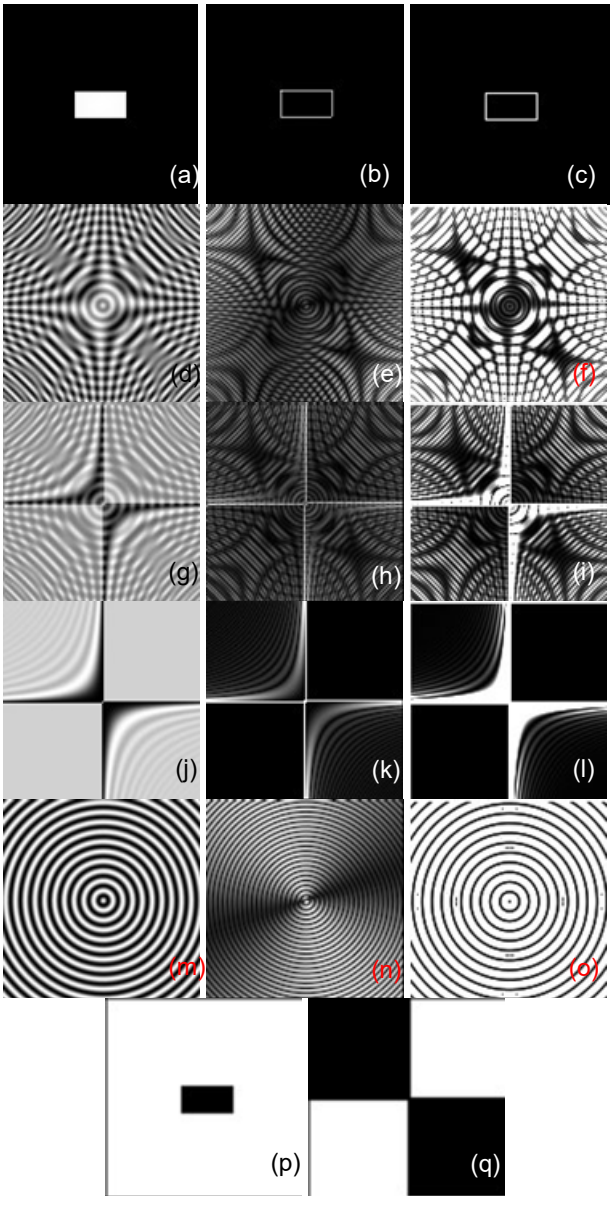

Note: The other SSD images were zero.

Figure 7 Magnetic resonance images in (a), (b), (c), (d) and (e); FODs calculated with h(x, y) in (f) and (i); FODs calculated with f(x, y) in (g), (h) and (j); FODs calculated with SRE2D in (k), (l), (m), (n) and (o)

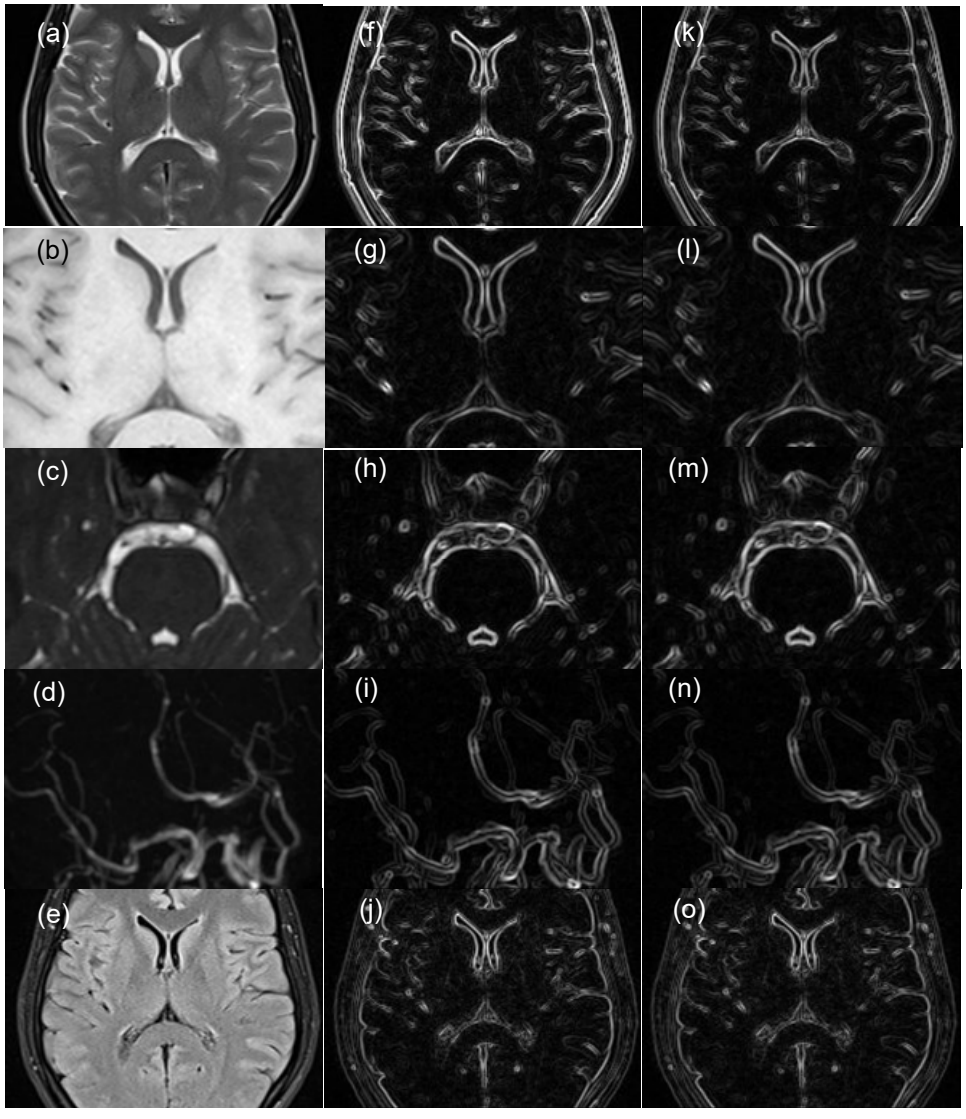

Results are presented in Figure 7 comparing performance of functions reported in the theory section, and in Figure 10 comparing the performance of bivariate linear model (SRE2D) and bivariate cubic model (B32D) (Yahaya, 2017). The FOD images were then direct Fourier transformed so to calculate the k-space magnitude and results are presented in Figures 8 and 11. Histograms of k-space magnitude images of FOD were calculated and plotted as shown in Figures 9 and 12. Average, standard deviation, and skewness of each histogram was calculated and reported in Tables 1 and 2. Value of statistics and t-tests indicate large degree of similarity between couple of histograms, which reflects the similarity between k-space images.

Figure 8 K-space magnitude images of the FOD displayed in Figure 7; (a), (b), (c), (d) and (e) are the k-space images of Figures 7(f), 7(g), 7(h), 7(i) and 7(j); (f), (g), (h), (i) and (j) are the k-space images of Figures 7(k), 7(l), 7(m), 7(n) and 7(o)

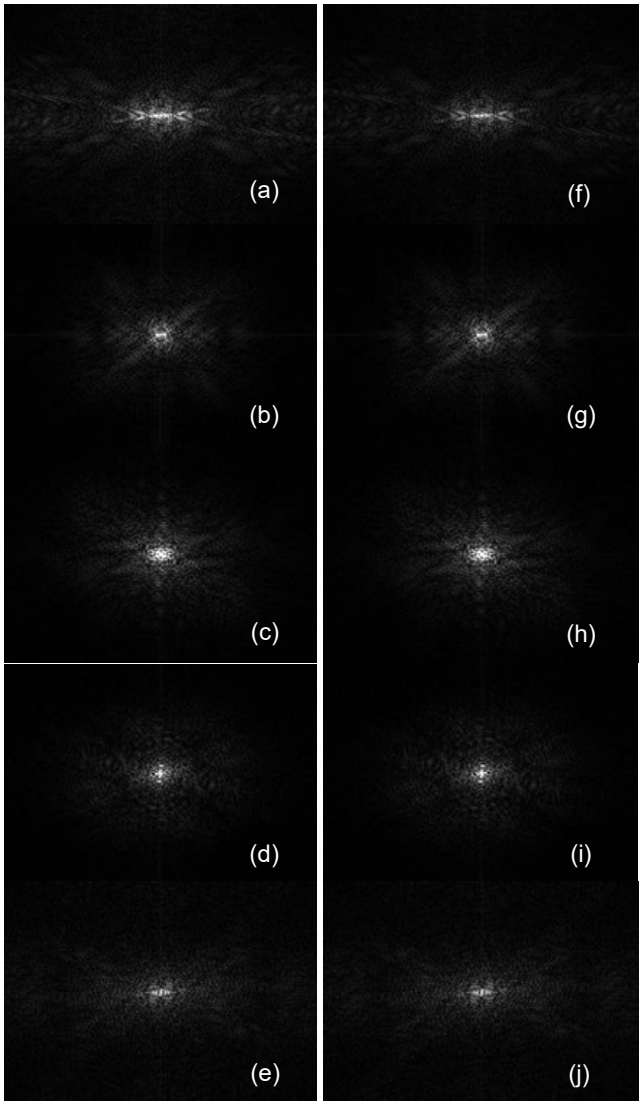

Each k-space image is representative of edge detection performance of FOD and thus representative of model function fitted to image data. The model functions and the derived FODs perform similarly. Such evidence is however clearly indicated by visual inspection of the images in Figures 7, 8, 10 and 11. Moreover, results in Figure 10 indicate that FOD calculated fitting bivariate linear model function (SRE2D) is sharper than FOD calculated fitting bivariate cubic polynomial (B32D). Sharpness is though accompanied by removal of background noise.

Figure 9 Histograms of k-space images displayed in Figure 8, (a), (b), (c), (d) and (e) are the histograms of Figures 8(a), 8(b), 8(c), 8(d) and 8(e) (f(x, y) and h(x, y) are the model polynomial functions); (f), (g), (h), (i) and (j) are the histograms of Figures 8(f), 8(g), 8(h), 8(i) and 8(j) (SRE2D is the model polynomial function) (see online version for colours)

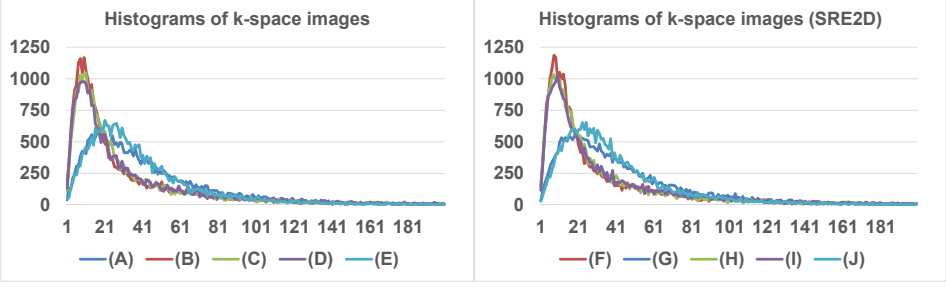

Figure 10 Magnetic resonance images in (a), (b), (c) and (d); FOD calculated with B32D model polynomial function (Yahaya, 2017) in (e), (f), (g) and (h); FOD calculated with SRE2D model polynomial function in (i), (j), (k) and (l)

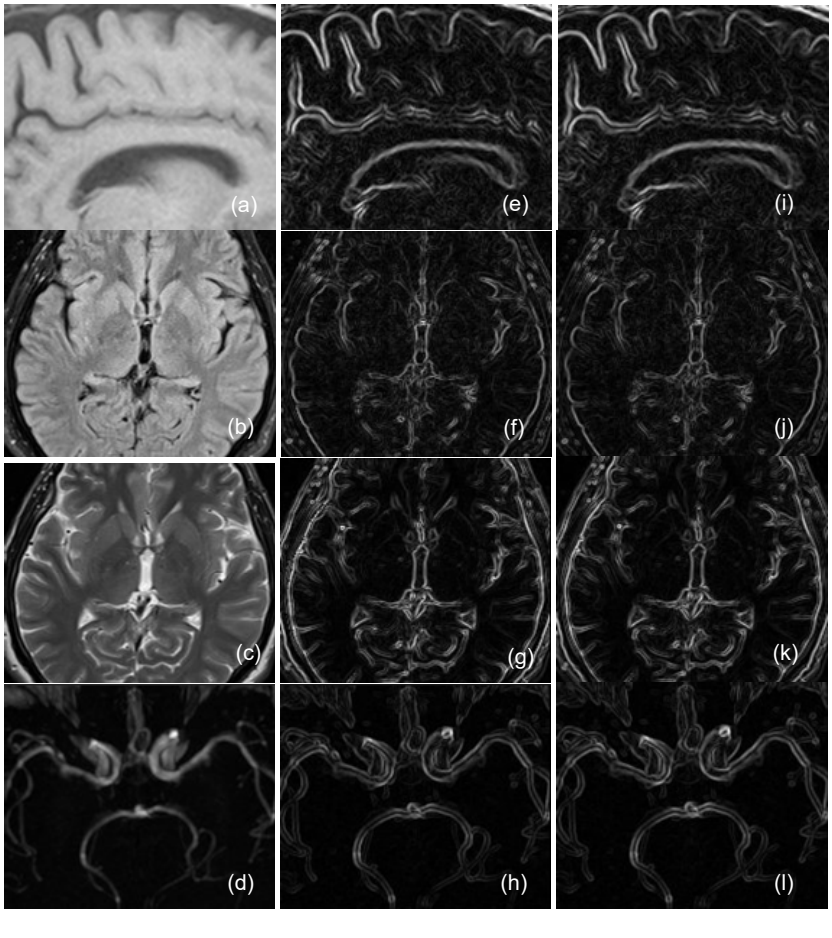

Figure 11 K-space magnitude images of the FOD displayed in Figure 10, (a), (b), (c) and (d) are the k-space images of Figures 10(e), 10(f), 10(g), 10(h); (e), (f), (g) and (h) are the k-space images of Figures 10(i), 10(j), 10(k), 10(l)

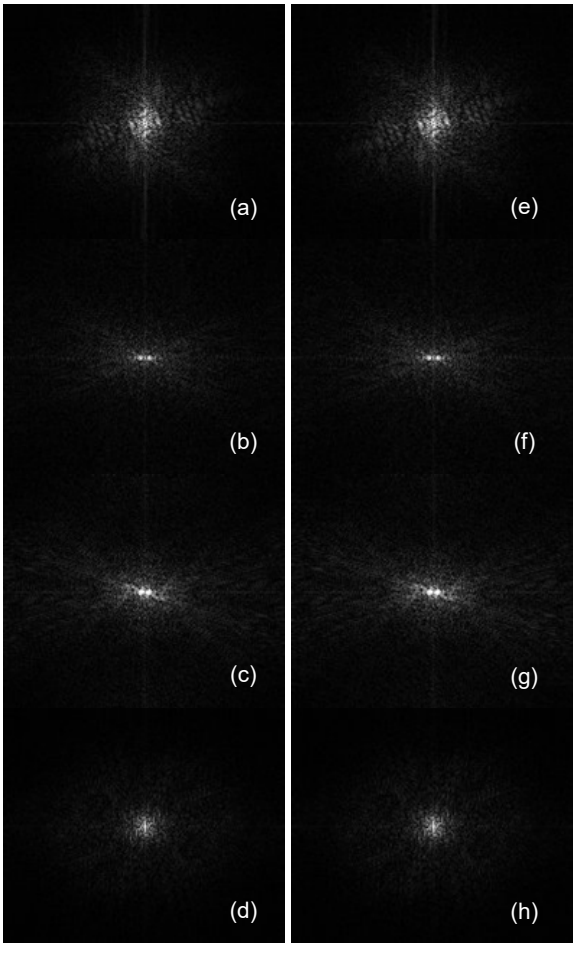

Figure 12 Histograms of k-space images displayed in Figure 11, (a), (b), (c), (d) are the histograms of Figures 11(a), 11(b), 11(c), 11(d) (B32D is the model polynomial function); (e), (f), (g), (h) are the histograms of Figures 11(e), 11(f), 11(g), 11(h) (SRE2D is the model polynomial function) (see online version for colours)

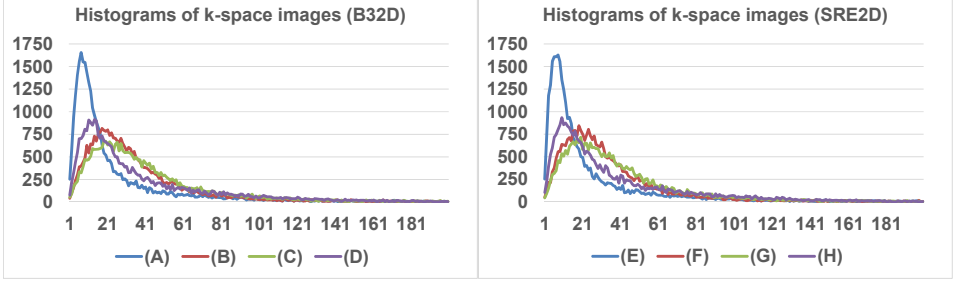

Figure 13 Comparison across methods (Spontón and Cardelino, 2015), (a) test magnetic resonance angiography, (b) SRE2D (our method), (c) Roberts, (d) Prewitt, (e) Sobel, (f) Haralick, (g) Marr-Hildreth (Gaussian kernel), (h) Marr-Hildreth (LoG kernel). Roberts, Prewitt and Sobel gradient threshold: 0.1 (see online version for colours)

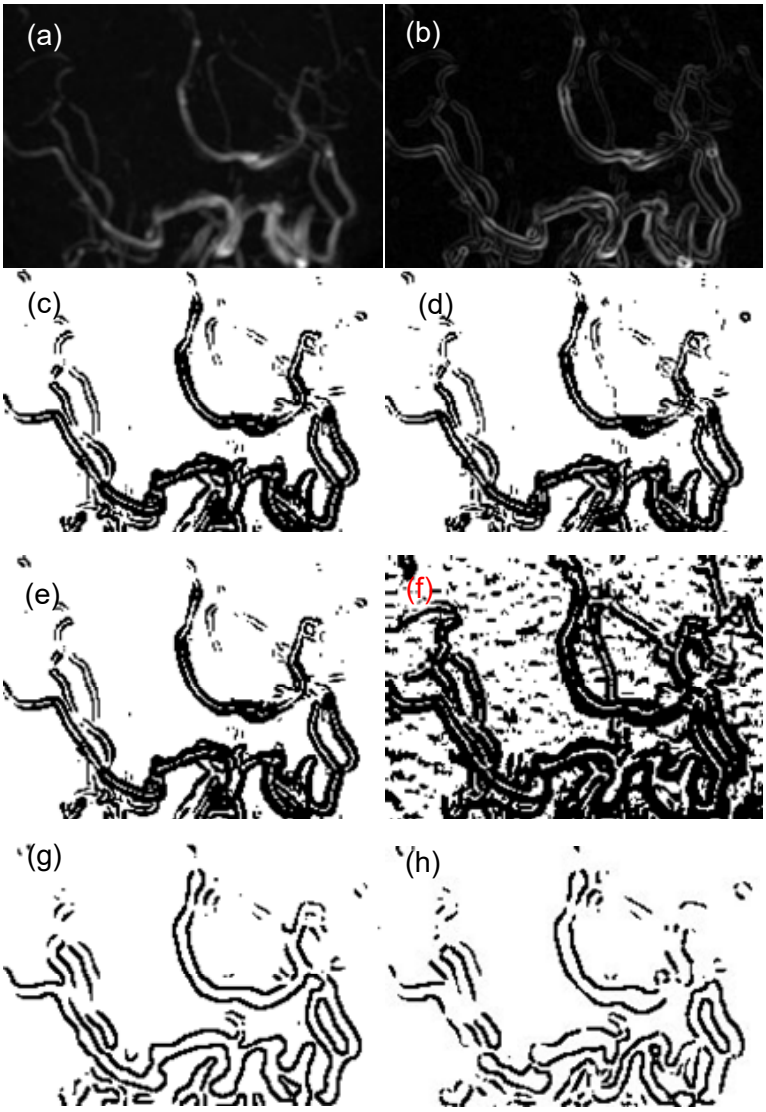

Notes: Haralick radius threshold from the centre of the pixel: 0.4. Marr-Hildreth (Gaussian kernel) blur standard deviation: 3, n (kernel size): 25; zero-crossing threshold: 0.07. Marr-Hildreth (LoG kernel) blur standard deviation: 3, n (kernel size): 29; zero-crossing threshold: 0.13. http://demo.ipol.im/demo/35/. The methods run over the internet connection in 0.79 sec. SRE2D runs in less than second too.

Table 1 Statistic values of the histograms displayed in Figure 9

Statistics	*(A)*	*(B)*	*(C)*	*(D)*	*(E)*
Skewness	1.1812	2.6221	2.3715	2.359	1.3684
Average	144.56	144.67	144.02	144.45	146.07
Std. dev.	169.21	253.23	240.01	228.71	192.5
Statistics	*(F)*	*(G)*	*(H)*	*(I)*	*(J)*
Skewness	1.1695	2.635	2.3649	2.3674	1.3453
Average	144.56	144.65	143.98	144.39	146.02
Std. dev.	168.9	252.93	240.17	228.73	191.33
t-test	1	0.999	0.998	0.997	0.997

Notes: Values are numerically close showing similarity of performance in edge detection of FOD of SRE2D and FOD of competing functions [see equations (2), (3), (4) and (5)]. The t-test throw additional evidence of similarity between FODs performance. The numerical values plotted in the histograms were scaled in the range [0, 255], however the raw images from which the histograms were calculated contain data in broader range represented through 64 bits real numbers.

Finally, Figure 13 displays comparison across methods. Magnetic resonance angiography in (a) is chosen to be the test image. The FOD calculated from SRE2D(x, y) model function [see (b)] is compared to Roberts, Prewitt, Sobel, Haralick and Marr-Hildreth methods. The figure legend reports on the parameters used to run the methods. FOD of SRE2D is able to visualise physiological connectivity of human brain vessels.

Table 2 Statistic values of histograms displayed in Figure 12

Statistics	*(A)*	*(B)*	*(C)*	*(D)*
Skewness	3.042	1.5658	1.3	1.94
Average	157.79	158.52	157.18	156.73
Std. dev.	332.66	231.44	201.27	223.02
Statistics	*(E)*	*(F)*	*(G)*	*(H)*
Skewness	3.0914	1.5745	1.3217	1.9378
Average	157.81	158.51	157.15	156.73
Std. dev.	334.32	234.04	204.84	223.06
t-test	0.999	0.999	0.998	1

Notes: Values are numerically close showing that edge detection performance of FOD of SRE2D and FOD of B32D are similar. The t-test adds more evidence in support to the similarity of performance. The numerical values plotted in the histograms were scaled in the range [0, 255], however the raw images from which the histograms were calculated contain data in broader range represented through 64 bits real numbers.

4 Discussion

4.1 The literature

Edge detection is a filtering technique that extracts the boundary between areas of an image characterised by different pixel brightness. The process of edge detection is

comparable to that one of a high pass filter because edges are spikes of high frequency signal. The process of unravelling edges of an image has been pivotal in machine vision, image understanding and image processing since when disciplines like computer vision exist (Jain et al., 1995; James, 2016). In the pioneering works found in the literature, edge detection process depends on differential operators which compute FODs, such as Canny, Roberts, Prewitt and Sobel operators (Roberts, 1963; Prewitt, 1979; Canny, 1986; Sobel, 1990), or second order derivatives such as Marr-Hildreth and Haralick operators (Marr and Hildreth, 1980; Haralick, 1984), and find zero crossing points across the image which target the boundary between objects and surfaces of the image (Spontón and Cardelino, 2015). Common approaches (such as Marr-Hildreth algorithm) also use Gaussian and Laplacian or, in alternative, Laplacian of the Gaussian (which calculates the second order derivative of the image), as smoothing preprocessing step; and then threshold achieves edge detection (Spontón and Cardelino, 2015). To calculate first and second order derivatives with convolutional filters, as described in the literature, is however quite different as opposed to pixel-by-pixel model polynomial fitting. Model polynomial fitting is proposed in this paper as the solution for the calculation of FOD, which turns into an edge detector when the departing polynomial includes spatial gradients. And, this is the case of all the model polynomials reported in this work including bivariate linear function SRE2D. Moreover, the use of convolutional filters such as Gaussian or Laplacian decreases dramatically the speed of computation because of the large number of numerical operations to be performed at the pre-processing step before threshold.

4.2 The novelty

This paper describes an approach to edge detection that is based on model polynomial fitting and calculation of FOD of the image. Model polynomial fitting makes this approach different from Roberts, Prewitt and Sobel operators, which approximates the FOD with convolutional masks (Roberts, 1963; Prewitt, 1979; Sobel, 1990); and closer to Haralick's (1984) approach that fits the data with discrete orthogonal polynomials. It has been observed in recent literature that the calculation of the FOD of an image on the basis of pixel-by-pixel fitting of model polynomial function yields excellent results as far as edge detection is concerned (Yahaya, 2017). Thus, motivated by the aforementioned results, this paper proposes the bivariate linear model function and a set of additional model polynomial functions. The paper evaluates edge detection properties of the function FODs across similar competing model functions designed with the specific purpose to compare edge detection characteristics. The FOD is defined by the square root of the sum of the squares of the first order partial derivatives of the model polynomial function fitted to the image data. The calculation of the FOD is carried out through calculus on a continuous function fitted to the image pixels. The calculation of first and second order partial derivatives of an image fitted with polynomials is also of recent inception, it yields to re-sampling techniques capable to extract information from images, and it has found a number of applications in MRI processing of the human brain (Ciulla, 2019a, 2019b, 2020; Ciulla and Agyapong, 2019). The key to edge detection property of the model function is the mathematical expression of gradients in the formula of the function. It is shown in this paper that three gradients (two along the principal coordinate directions 'x' and 'y', and one that covers the covariate 'xy' direction) are sufficient to determine effective edge detection properties of the FOD of the model functions.

4.3 Conclusions

All of the model polynomial functions presented in this paper were found to have similar edge detection behaviour. The reason and the key to the successful performance of edge detection using model polynomial fitting to the image, is to design the function with three gradients: one for each spatial direction and one for the covariate direction. In addition, the polynomial functions here reported are parametric in the constants ‘a’, ‘b’ and ‘c’. To obtain optimal performance, it was observed that the value of the constants needs to be the same. Indeed by doing so, the three gradients are equally active and can equally detect edges along the three aforementioned directions. Moreover, the value of the constants can be kept reasonably small (inside the range [–2.5, 2.5]). In conclusion, a computationally fast approach to edge detection in two-dimensional images has been presented. It is based on model polynomial fitting, and as evaluated across the spectrum of five model functions, it shows a viable option for edge detection. Future work might assess the relative contribution to edge finding behaviour of the gradients of each model function and determine an overall optimal function for edge detection using its FOD.

Contributions

GM, NS, SD and NZ, studied the polynomial functions reported in the theory section. They implemented the code in C++ and collected the results. CC calculated the k-space of the FOD images, their histograms and the value of the statistics. CC also wrote the paper. The students participated actively to the final review of the paper. This paper is a learning experience initiated by the teacher (CC) with the specific aim to facilitate the introduction in STEM disciplines of participating students for their future endeavours. The teacher is the main contributor to the article, however his name appears as third author because the article wants to witness the efforts spent by the four students in compiling their bachelor degree theses.

Lessons learned

We have initially believed that to parameterise the model functions with the constants ‘a’, ‘b’ and ‘c’ would yield to endless flexibility of edge detection properties of the FODs. However, we have learned that the optimal results in edge detection are obtained keeping the constants in the range [–2.5, 2.5]. Moreover, to equally use the three gradients of the model functions, the constants can be set to the same value, ensuring equity in edge detection along the two spatial coordinates ‘x’, ‘y’ and the covariate direction ‘xy’.

Ethics

MRI acquisition was consented and approval was obtained from subjects to use the images for research after the administration of written consent. This study was conducted according to principles expressed in the 1964 Declaration of Helsinki.

Disclaimer

No funding was received to support this research.

Acknowledgements

Hereto publishing findings that benefit from OASIS (http://www.oasis-brains.org/) data (see MRI in Figure 1). The authors are due to mention the following grant numbers: P50 AG05681, P01 AG03991, R01 AG021910, P50 MH071616, U24 RR021382, R01 MH56584. The authors express sincere gratitude to Dr. Dimitar Veljanovski and Dr. Filip A. Risteski because of the availability of the additional MR images and also to Professor Ustijana Rechkoska Shikoska for the help provided to coordinate the human resources. Dr. Dimitar Veljanovski and Dr. Filip A. Risteski are affiliated with the Department of Radiology, General Hospital 8-mi Septemvri, Boulevard 8th September, Skopje, 1000, Republic of North Macedonia. Professor Ustijana Rechkoska Shikoska is affiliated with the University of Information Science and Technology (UIST), Partizanska BB, Ohrid, 6000, Republic of North Macedonia. The magnetic resonance angiography images were provided by the corresponding author.

References

Bryan, R.N., Davatzikos, C., Herskovits, E.H., Mohan, S., Rudie, J.D. and Rauschecker, A.M. (2020) 'Medical image analysis: human and machine', *Academic Radiology*, Vol. 27, No. 1, pp. 76-81.

Canny, J. (1986) 'A computational approach to edge detection', *IEEE Transactions on Pattern Analysis and Machine Intelligence*, Vol. PAMI-8, No. 6, pp.679–698.

Caviedes, J. and Gurbuz, S. (2002) 'No-reference sharpness metric based on local edge kurtosis', *Proceedings of IEEE International Conference on Image Processing*, NY, USA, pp.3: III-53–III-56.

Ciulla, C. (2019a) 'Intensity-curvature functional-based filtering in image space and in k-space: applications in magnetic resonance imaging of the human brain', *High Frequency*, Vol. 2, No. 1, pp.48–60.

Ciulla, C. (2019b) 'The use of the intensity-curvature measurement approaches: applications in magnetic resonance imaging of the human brain', *Engineering Reports*, Vol. 1, No. 5, p.e12063.

Ciulla, C. (2020) 'Combined inverse Fourier transformation of magnetic resonance and intensity-curvature functional images', *Engineering Reports*, p.e12290, https://doi.org/ 10.1002/eng2.12290.

Ciulla, C. and Agyapong, G. (2019) 'Intensity-curvature functional based digital high pass filter of the bivariate cubic B-spline model polynomial function', *Visual Computing for Industry, Biomedicine, and Art*, Vol. 2, No. 9, https://vciba.springeropen.com/articles/10.1186/ s42492-019-0017-6.

Ciulla, C., Risteski, F.A., Veljanovski, D., Rechkoska, U.S., Adomako, E. and Yahaya, F. (2015) 'A compilation on the contribution of the classic-curvature and the intensity-curvature functional to the study of healthy and pathological MRI of the human brain', *Int. J. Applied Pattern Recognition*, Vol. 2, No. 3, pp.213–234.

Cosgrove, C. and Yuille, A. (2020) 'Adversarial examples for edge detection: they exist, and they transfer', in *The IEEE Winter Conference on Applications of Computer Vision*, pp.1070–1079.

Dolz, J., Massoptier, L. and Vermandel, M. (2015) 'Segmentation algorithms of subcortical brain structures on MRI for radiotherapy and radiosurgery: a survey', *IRBM – Innovation and Research in Biomedical Engineering*, Vol. 36, No. 4, pp.200–212.

Haralick, R.M. (1984) 'Digital step edges from zero crossing of the second directional derivatives', *IEEE Transactions on Pattern Analysis and Machine Intelligence*, Vol. 1, No. 6, pp.58–68.

He, J., Zhang, S., Yang, M., Shan, Y. and Huang, T. (2019) 'Bi-directional cascade network for perceptual edge detection', in *Proceedings of the IEEE Conference on Computer Vision and Pattern Recognition (CVPR)*, June, pp.3828–3837.

Jain, R., Kasturi, R. and Schunck, B.G. (1995) *Machine Vision*, Vol. 5, pp.309–364, McGraw-Hill, New York.

James, A.P. (2016) 'Edge detection for pattern recognition: a survey', *Int. J. Applied Pattern Recognition*, Vol. 3, No. 1, pp.1–21.

Khin, T., Srujan Raju, K., Sinha, G.R., Khaing, K.K. and Kyi, T.M. (2020) 'Review of optimization methods of medical image segmentation', in Raju, K., Govardhan, A., Rani, B., Sridevi, R. and Murty, M. (Eds.): *Proceedings of the Third International Conference on Computational Intelligence and Informatics: Advances in Intelligent Systems and Computing*, Springer, Singapore, Vol. 1090, pp.213–218.

Liu, Y., Cheng, M.M., Hu, X., Wang, K. and Bai, X. (2017) 'Richer convolutional features for edge detection', in *Proceedings of the IEEE Conference on Computer Vision and Pattern Recognition*, pp.3000–3009.

Marr, D. and Hildreth, E.C. (1980) 'Theory of edge detection', *Proceedings of the Royal Society of London Biological Sciences*, Vol. 207, No. 1167, pp.187–217.

Prewitt, J.M.S. (1970) 'Object enhancement and extraction', in Lipkin, B.S. and Rosenfeld, A. (Eds.): *Picture Processing and Psychopictorics*, pp.75–149, Academic Press, New York.

Ren, H., Zhao, S. and Gruska, J. (2018) 'Edge detection based on single-pixel imaging', *Optics Express*, Vol. 26, No. 5, pp.5501–5511.

Roberts, L.G. (1963) *Machine Perception of Three-Dimensional Solids*, PhD thesis, Massachusetts Institute of Technology, USA.

Sadykova, D. and James, A.P. (2017) 'Quality assessment metrics for edge detection and edge-aware filtering: a tutorial review', in *IEEE International Conference on Advances in Computing, Communications and Informatics (ICACCI)*, pp.2366–2369.

Sobel, I. (1990) 'An isotropic 3 × 3 image gradient operator', in Freeman, H. (Ed.): *Machine Vision for Three-Dimensional Scenes*, pp.376–379, Academic Press.

Spontón, H. and Cardelino, J. (2015) 'A review of classic edge detectors', *Image Processing on Line*, Vol. 5, pp.90–123 [online] http://www.ipol.im/pub/art/2015/35/?utm_source=doi.

Wang, M. and Li, P. (2019) 'A review of deformation models in medical image registration', *Journal of Medical and Biological Engineering*, Vol. 39, No. 1, pp.1–17.

Xie, S. and Tu, Z. (2015) 'Holistically-nested edge detection', in *Proceedings of the IEEE International Conference on Computer Vision (ICCV)*, pp. 139–1403.

Yahaya, F. (2017) 'Edge finding in magnetic resonance imaging applications: the calculation of the first order derivative of two dimensional images', *Int. J. Applied Pattern Recognition*, Vol. 4, No. 3, pp.226–245.

Zhang, W., Zhao, Y., Breckon, T.P. and Chen, L. (2017) 'Noise robust image edge detection based upon the automatic anisotropic Gaussian kernels', *Pattern Recognition*, Vol. 63, No. 8, pp.193–205, https://dro.dur.ac.uk/20599/; https://dro.dur.ac.uk/cgi/export/20599/BibTeX/dur-eprint-20599.bib.

Zhao, Z.Q., Zheng, P., Xu, S.T. and Wu, X. (2019) 'Object detection with deep learning: a review', *IEEE Transactions on Neural Networks and Learning Systems*, Vol. 30, No. 11, pp.3212–3232.